J. Fluid Mech. (2013), *vol.* 727, *pp.* 379–406.
doi:10.1017/jfm.2013.217

Invariants for slightly heated decaying grid turbulence

R. A. Antonia[1], S. K. Lee[1], L. Djenidi[1,†], P. Lavoie[2] and L. Danaila[3]

[1]School of Engineering, University of Newcastle, NSW, 2308, Australia
[2]Institute for Aerospace Studies, University of Toronto, ON, Canada M3H 5T6
[3]CORIA CNRS UMR 6614, Université de Rouen, 77801 Saint Etienne du Rouvray, France

(Received 19 September 2012; revised 18 April 2013; accepted 23 April 2013;
first published online 26 June 2013)

The paper examines the validity of velocity and scalar invariants in slightly heated and approximately isotropic turbulence generated by passive conventional grids. By assuming that the variances $\langle u^2\rangle$ and $\langle\theta^2\rangle$ (u and θ represent the longitudinal velocity and temperature fluctuations) decay along the streamwise direction x according to power laws $\langle u^2\rangle \sim (x-x_0)^{n_u}$ and $\langle\theta^2\rangle \sim (x-x_0)^{n_\theta}$ (x_0 is the virtual origin of the flow) and with the further assumption that the one-point energy and scalar variance budgets are represented closely by a balance between the rates of change of $\langle u^2\rangle$ and $\langle\theta^2\rangle$ and the corresponding mean energy dissipation rates, the products $\langle u^2\rangle\lambda_u^{-2n_u}$ and $\langle\theta^2\rangle\lambda_\theta^{-2n_\theta}$ must remain constant with respect to x. Here λ_u and λ_θ are the Taylor and Corrsin microscales. This is unambiguously supported by previously available data, as well as new measurements of u and θ made at small Reynolds numbers downstream of three different biplane grids. Implications for invariants based on measured integral length scales of u and θ are also tested after confirming that the dimensionless energy and scalar variance dissipation rate parameters are approximately constant with x. Since the magnitudes of n_u and n_θ vary from grid to grid and may also depend on the Reynolds number, the Saffman and Corrsin invariants which correspond to a value of -1.2 for n_u and n_θ are unlikely to apply in general. The effect of the Reynolds number on n_u is discussed in the context of published data for both passive and active grids.

Key words: homogeneous turbulence, isotropic turbulence, turbulence theory

1. Introduction

An important objective in turbulence research is to predict statistical quantities at the simplest level (or the lowest order). For decaying homogeneous isotropic turbulence, a long-standing issue has been the prediction of the rate of decay of the kinetic energy, i.e. the prediction of the exponent n_u when $\langle u^2\rangle \sim (x-x_0)^{n_u}$. Experimental and numerical results lead to a relatively wide range of values for n_u. Our understanding of these values, as a function of different initial conditions, requires analytical developments that establish a link between n_u and quantities called invariants, which in essence reflect the permanence of the big eddies and remain constant throughout the decay. In an experimental context, the term 'initial conditions'

† Email address for correspondence: lyazid.djenidi@newcastle.edu.au

refers to the flow conditions immediately upstream of the grid, the geometry and dimensions of the grid and the Reynolds number at the grid. In the majority of the numerical simulations that have been performed, the effect of initial conditions is set by the slope of the initially assumed energy spectrum as the wavenumber k approaches zero.

1.1. *Brief history on the permanence of big eddies*

Kolmogorov (1941) obtained a simple prediction for the initial period of decay of isotropic turbulence based on the following assumptions (here we use the distance x from the grid instead of the time t to allow direct comparison with grid turbulence).

(A1) The Loitsyansky (1939) integral is constant, namely

$$I_4 = \int_0^\infty r^4 \langle u(x)u(x+r)\rangle \, \mathrm{d}r = \text{constant}, \tag{1.1}$$

where $\langle u(x)u(x+r)\rangle$ is the two-point longitudinal velocity correlation; u is the velocity fluctuation in the x direction and the angular brackets denote time averaging. The subscript '4' denotes the power exponent of the scale r.

(A2) The velocity correlation function at large r is self-similar with a length scale that is proportional to the integral length scale L, namely

$$\langle u(x)u(x+r)\rangle = \langle u^2\rangle f(r/L). \tag{1.2}$$

(A3) The mean energy dissipation rate $\langle\epsilon\rangle$ is related to L, namely

$$C_\epsilon = \frac{\langle\epsilon\rangle L}{\langle u^2\rangle^{3/2}} \sim \text{constant}. \tag{1.3}$$

Relation (1.3) is based on the assumption that the Taylor microscale Reynolds number $R_{\lambda_u} = \langle u^2\rangle^{1/2}\lambda_u/\nu$, where $\lambda_u = (\langle u^2\rangle/\langle(\partial u/\partial x)^2\rangle)^{1/2}$ is the Taylor microscale associated with u and ν is the kinematic viscosity, is large enough to produce an inertial subrange (Kolmogorov 1941) so that $\langle u(x)u(x+r)\rangle/\langle u^2\rangle \sim 1 - \langle\epsilon\rangle^{2/3} r^{2/3}/\langle u^2\rangle$. However, Sreenivasan (1984) indicated that C_ϵ may be constant at relatively small values of R_{λ_u} ($\gtrsim 50$) although the possibility that it depends on initial conditions could not be ruled out (Sreenivasan 1998). This possibility was confirmed by Burattini, Lavoie & Antonia (2005), who further showed that, for direct numerical simulations (DNS) of box turbulence, C_ϵ appears to be constant for $R_{\lambda_u} \gtrsim 200$. Also, it should be noted that for turbulence generated by a class of multiscale grids (Valente & Vassilicos 2011), C_ϵ is not constant.

By combining (1.1) and (1.2), it follows that

$$\langle u^2\rangle L^5 = \text{constant}, \tag{1.4}$$

provided the integral $A_L = \int_0^\infty (r/L)^4 f(r/L)\, \mathrm{d}(r/L)$ is constant during the decay. For grid turbulence, the transport equation for $\langle u^2\rangle$ is given, to a close approximation, by

$$\langle\epsilon\rangle = -\frac{3}{2} U_0 \frac{\mathrm{d}\langle u^2\rangle}{\mathrm{d}x}, \tag{1.5}$$

where U_0 is the constant local mean velocity. It follows from (1.3)–(1.5) that $\langle u^2\rangle$ and L exhibit the power-law variations

$$\langle u^2\rangle \sim (x - x_0)^{-10/7}, \quad L \sim (x - x_0)^{2/7}. \tag{1.6}$$

A more general derivation of Kolmogorov's decay law is given by Frisch (1995, §7.7). He enunciated the principle of permanence of large eddies which, in Fourier space, states essentially that if initially the energy spectrum behaves as $E(k) \sim C'k^s$ (for $k \to 0$) with

$$s = -\frac{2+3n_u}{2+n_u}, \tag{1.7}$$

then this property will hold at later times with the same s.

Batchelor (1948) obtained the relations (1.6) via a complete self-preserving solution of the inviscid (high R_{λ_u}) Kármán & Howarth (1938) (K–H) equation; the ratio L/λ_u was allowed to vary with x. Batchelor assumed (1.1) but did not use (1.3), although (1.3) is satisfied by (1.5) and (1.6).

Comte-Bellot & Corrsin (1966) indicated that since (1.1) does not hold (see also Proudman & Reid (1954) and Batchelor & Proudman (1956)), relations (1.6) have not received much attention. They noted that the decay exponent '$-10/7$' is smaller than their values (-1.15 to -1.33) obtained for different grids with the use of a secondary contraction to improve the isotropy at the large scales.

Saffman (1967*a*,*b*) confirmed Birkhoff's (1954) speculation that Loitsyansky's integral is in general divergent and that it exists only for a restricted type of isotropic turbulence. For isotropic turbulence at large R_{λ_u}, Saffman proposed

$$I_2 = \int_0^\infty r^2 R(r)\,\mathrm{d}r = \text{constant}, \tag{1.8}$$

where $R(r)$ is the trace of the 2-point velocity correlation tensor. Using (1.2) and (1.3), and observing (1.5), it follows that

$$\langle u^2\rangle \sim (x-x_0)^{-6/5}, \quad L \sim (x-x_0)^{2/5}, \tag{1.9}$$

where (1.4) is now replaced by

$$\langle u^2\rangle L^3 = \text{constant}. \tag{1.10}$$

The idea that I_2 is conserved has been challenged by Davidson (2000, 2009) who concluded that, for certain initial conditions, freely evolving turbulence can reach an asymptotic state in which the variation of I_2 is negligible. Numerical simulations (Ishida, Davidson & Kaneda 2006) of decaying turbulence with a domain much larger than L and with $E(k \to 0) \sim k^4$ as a prescribed initial condition, indicate that it may be possible to reach a state characterized by $I_4 = \text{constant}$ with $\langle u^2\rangle \sim t^{-10/7}$. This would support Davidson's (2000) idea that long-range pressure forces may not be important and that the general impression that I_2 could not be conserved is in part due to a misinterpretation of the analysis of Batchelor & Proudman (1956).

Equation (1.7) indicates that when the slope s of the spectrum ($k \to 0$) assumes values of 4 and 2, the corresponding values of n_u are $-10/7$ and $-6/5$, as given by (1.6) and (1.9). The value $s = 1$ corresponds to $n_u = -1$, the decay exponent expected for very large R_{λ_u} (this is discussed in the following subsection). It is generally believed that the decay exponent should be influenced, at least in the initial period of decay, by the large-scale motion or the manner in which the spectrum behaves at low wavenumbers. In spite of the result obtained by Ishida *et al.* (2006) and leaving aside the case $s = 1$, the DNS of Huang & Leonard (1994), who used initial spectra with either $s = 4$ or $s = 2$, imply that there is little, if any, correlation between s and n_u, the latter tending to depend rather on $R_\lambda(t = 0)$. The DNS results of Antonia & Orlandi (2004), where the initial spectrum was chosen to have the same form as that used by

Huang & Leonard (1994) and Mansour & Wray (1994) yielded a value of n_u close to -1.1 even though s was set equal to 4.

For a 'conventional' grid made of a sheet-metal plate with perforated square holes, which is different from the biplane square grid of Comte-Bellot & Corrsin (1966) and Lavoie, Djenidi & Antonia (2007), Krogstad & Davidson (2010) obtained a decay exponent of -1.13 for $\langle q^2\rangle$ ($\langle q^2\rangle = \langle u^2\rangle + \langle v^2\rangle + \langle w^2\rangle$ is the total kinetic energy). The deviation from $-6/5$ was ascribed to a slight departure from constancy (with respect to (w.r.t.) x) of C_ϵ. Also, Krogstad & Davidson (2011) studied the turbulence downstream of two multiscale grids and found that, once homogeneity is established, the decay exponent is slightly closer to $-6/5$ than for their conventional grid. Krogstad & Davidson (2011) concluded that there is no significant difference in the behaviour between the three grids, notwithstanding the different initial conditions, reinforcing the idea that grid turbulence satisfies (1.9) and (1.10).

This conclusion, however, was contested by Valente & Vassilicos (2012) who reanalysed the data of Krogstad & Davidson (2010, 2011) and found that in fact the exponent of L in (1.10) is larger than 3, varying between 3.7 and 4.4, underlining the expectation that initial conditions matter.

At first sight, all of these studies seem to indicate that neither $I_4 = \text{constant}$ nor $I_2 = \text{constant}$ have strong claims to generality, at least for the grid flows that have been examined in the literature.

There are two possible explanations for the fact that these invariants are not conserved.

(i) The possibility that $\langle u^2\rangle L^{\alpha_u}$ is an invariant (with $\alpha_u \equiv m+1$ not necessarily equal to 3 or 5) has been discussed (Llor 2011; Vassilicos 2011). It is straightforward to infer that $n_u = -2\alpha_u/(2+\alpha_u)$. Relations (1.4) and (1.10) correspond to $n_u = -10/7$ and $-6/5$, respectively. This brings us to a broader context of invariants I_m, with m not necessarily equal to 2 or 4.

(ii) The possibility that not only does the power law α_u of $\langle u^2\rangle L^{\alpha_u}$ vary from flow to flow, but the scale involved in this relation may also differ from the integral scale L. Both of these scenarios are considered in § 1.2.

1.2. *The general context of invariants at any order*

The possibility of the existence of an infinite number of invariants has been mathematically demonstrated by Vassilicos (2011). The initial point of departure is that quantities such as

$$I_m = \int_0^\infty r^m \langle u(x)u(x+r)\rangle \,\mathrm{d}r, \tag{1.11}$$

remain constant during the decay. This can be reduced to two mathematical requirements, which must be satisfied simultaneously, namely

$$\int_0^\infty (r/l)^m \langle u(x)u(x+r)\rangle/\langle u^2\rangle \,\mathrm{d}(r/l) = \text{constant}, \tag{1.12}$$

$$\langle u^2\rangle l^{m+1} = \text{constant}, \tag{1.13}$$

where l is the self-preserving scale.

We should first note that (1.12) represents a weak formulation of the complete self-preservation requirement, $f(r/l) = \text{constant}$ w.r.t. x, where f represents the normalized two-point correlation. In other words, if $f(r/l) = \text{constant}$ w.r.t. x, then $(r/l)^m f(r/l) = \text{constant}$ w.r.t. x and, hence, the integral from 0 to ∞ of this quantity is

conserved, $\forall m$. Yet, the next obvious question is what is l? Kolmogorov indicated that, as far as the invariant I_4 is concerned, the most adequate scale is the integral scale L. As already discussed in § 1.1, many studies have been devoted to the 'permanence of big eddies' and the associated invariants, i.e. those involving the integral scale L. Since there has only been equivocal support for this approach, the question of what is the appropriate choice for l remains open.

It is pertinent to recall here that since l should be the similarity scale for f whose dynamics is described by the Kármán–Howarth equation, one could argue that l may be more suitably represented by the Taylor microscale, λ_u, than by L. Indeed, George (1992*a*,*b*) proposed an equilibrium similarity solution, valid for any Reynolds number: the kinetic energy decays as $\langle u^2\rangle \sim (x-x_0)^{n_u}$, with n_u determined by the initial conditions, and the self-similarity length scale is λ_u.

George's solution was tested in physical space for small R_{λ_u} grid turbulence by Antonia *et al.* (2003) via the transport equation for $\langle(\delta q)^2\rangle$. Here, $\langle(\delta q)^2\rangle = \langle(\delta u)^2\rangle + \langle(\delta v)^2\rangle + \langle(\delta w)^2\rangle$ and $\delta\psi = \psi(x+r) - \psi(x)$ is a velocity (or scalar) increment; $\psi \equiv u,\ v,\ w$ (or θ). The measurements of $\langle(\delta q)^2\rangle$ and $\langle(\delta u \delta q)^2\rangle$ satisfied similarity fairly closely over a wide range of r/λ_u, where r is the separation between the two points (Antonia *et al.* 2003). At small r, Kolmogorov scaling was more appropriate (Antonia & Orlandi 2004) while at large r, when $\langle(\delta u \delta q)^2\rangle$ is negligible, the integral length scale becomes more relevant. Speziale & Bernard (1992) noted that George's solution is incomplete at least for small values of R_{λ_u} usually achieved in the majority of passive grid turbulence experiments. Nonetheless, it is of interest since a family of incomplete self-preserving states appears possible, each state corresponding to a given set of initial conditions.

Speziale & Bernard (1992) used a fixed-point analysis and numerical integration of exact one-point transport equations for the mean energy and energy dissipation rate to show that $n_u = -1$ is the asymptotically consistent high-R_{λ_u} solution and represents the state towards which a complete self-preserving isotropic turbulence is driven. An analytical derivation of this result is given by Ristorcelli (2003) whilst numerical support for the x^{-1} decay rate was provided by Lesieur & Schertzer (1978) and Lesieur & Ossia (2000). Speziale & Bernard (1992) found that the Taylor microscale λ_u is the only similarity length scale that can yield complete self-preserving solutions to the full viscous equations of motion for isotropic turbulence. Speziale & Bernard (1992) also indicated that $n_u = -6/5$ is not consistent with a complete self-preserving solution to the inviscid K–H equation.

In the light of the above-mentioned studies, there is support for λ_u as the relevant self-preserving scale. Note however that, for the weaker requirement $(r/l)^m f(r/l) =$ constant w.r.t. x, and for large values of m, the behaviour of f at large scales is increasingly important, thus leaving open the possibility that the integral scale L may be the appropriate self-preserving scale.

Experimentally, it is difficult to check the constancy w.r.t. x of I_m since the integrands are unlikely to approach zero in a smooth fashion due in part to the lack of convergence of the correlations at large r and also to the adverse effect of the test section boundaries on these correlations. Wang & George (2002) have suggested that almost all reported integral scales in isotropic turbulence are questionable.

As far as (1.13) is concerned, it can be more easily tested with experimental data. Given an adequate expression of the scale l, the aim is to find the value of the exponent $\alpha_u^l \equiv m+1$ so that $\langle u^2\rangle l^{\alpha_u^l} =$ constant during the decay. The notation α_u^l

indicates that the invariant $\langle u^2\rangle l^{\alpha_u^l}$ (involving the velocity component u and the scale l) holds.

1.3. *Our approach*

As already underlined, the tests carried out in the present paper, like those of Krogstad & Davidson (2010, 2011) and Valente & Vassilicos (2012) simply focus on relations (1.13) rather than on (1.12).

More generally, we ask the question, similar to that posed by George (1992*a*,*b*): what is the optimum value of α_u^L which corresponds to a particular value of n_u and therefore a particular set of initial conditions?

The starting point is the one-point kinetic energy budget (1.5), together with the assumption that $\langle u^2\rangle$ decays according to a power law. It follows that $\langle\epsilon\rangle \sim (x-x_0)^{n_u-1}$. By recalling that $\lambda_u^2 \sim \langle u^2\rangle/\langle\epsilon\rangle$, it is straightforward to deduce that

$$\lambda_u^2 \sim x - x_0. \tag{1.14}$$

Therefore, there is an immediate invariant which involves the Taylor microscale, i.e.

$$\langle u^2\rangle \lambda_u^{\alpha_u^\lambda} = \text{constant}, \tag{1.15}$$

with

$$\alpha_u^\lambda = -2n_u. \tag{1.16}$$

Equation (1.15) represents one possible form of (1.13), which does not require any particular assumption about the large scales. Note that the assumptions underlying (1.15) have received strong experimental support (George 1992*b*; Antonia *et al.* 2003). Also the emergence of λ_u as the relevant length scale of the invariants is not inconsistent with the support that the λ_u-based equilibrium similarity of George (1992*b*) has received in both spectral and physical spaces.

Developing possible invariants involving the integral scale L requires the connection between λ_u and L to be established. This can be done by assuming that Equation (1.3) holds. It follows that

$$\frac{L}{\lambda_u} \sim R_{\lambda_u}, \tag{1.17}$$

and for the following invariant to be valid

$$\langle u^2\rangle L^{\alpha_u^L} = \text{constant}, \tag{1.18}$$

it is necessary that (Vassilicos 2011)

$$n_u = -\frac{2\alpha_u^L}{2+\alpha_u^L}, \tag{1.19a}$$

$$\alpha_u^L = -\frac{2n_u}{2+n_u}. \tag{1.19b}$$

1.4. *Extension to the passive scalar field*

The extension of Kolmogorov's (1941) prediction to the scalar field is straightforward. The following assumptions are needed.

(B1) The Corrsin (1951) integral is constant, namely

$$I_{2\theta} = \int_0^\infty r^2 \langle\theta(x)\theta(x+r)\rangle \,\mathrm{d}r = \text{constant}, \tag{1.20}$$

where θ denotes the scalar fluctuation and $\langle\theta(x)\theta(x+r)\rangle$ is the two-point scalar correlation; $I_{2\theta}$ is analogous to I_4 (Corrsin 1951) or more correctly, it is analogous to I_2 (Hinze 1975, p. 288), i.e. if the velocity characteristics of grid turbulence are Saffman-like, the scalar characteristics are Corrsin-like.

(B2) The scalar-correlation function is self-similar, namely

$$\langle\theta(x)\theta(x+r)\rangle = \langle\theta^2\rangle f_\theta(r/L_\theta), \tag{1.21}$$

where $\langle\theta^2\rangle$ is the scalar variance and L_θ is the integral length scale of θ.

From (1.20) and (1.21), together with the assumption that the normalized scalar dissipation rate is constant, we obtain (with $\xi = L/L_\theta = 1$)

$$\langle\theta^2\rangle L^3 = \text{constant}. \tag{1.22}$$

By using (1.22) and the transport equation for $\langle\theta^2\rangle$, namely

$$\langle\chi\rangle = -\frac{U_0}{2}\frac{\mathrm{d}\langle\theta^2\rangle}{\mathrm{d}x}, \tag{1.23}$$

we arrive at (with $\xi = 1$)

$$\langle\theta^2\rangle \sim (x - x_0)^{-6/5}, \quad L \sim x^{2/5}. \tag{1.24}$$

That (1.22) and (1.24) are similar to (1.9) and (1.10) is not surprising in view of the similarity between the transport equations for $\langle\boldsymbol{q}(x)\boldsymbol{q}(x+r)\rangle$ and $\langle\theta(x)\theta(x+r)\rangle$ (Rey *et al.* 1976; Fulachier & Antonia 1984) ($\boldsymbol{q}$ is the velocity vector $u\boldsymbol{i} + v\boldsymbol{j} + w\boldsymbol{k}$, where u, v and w are the velocity fluctuations in the x, y and z directions, respectively) or between the transport equations for $\langle(\delta q)^2\rangle$ and $\langle(\delta\theta)^2\rangle$ (Antonia *et al.* 1996, 1997; Danaila *et al.* 1999). This similarity, which is reflected in the analogy between the Saffman and Corrsin invariants or in the analogous forms of the inhomogeneous terms in the transport equations for $\langle(\delta q)^2\rangle$ and $\langle(\delta\theta)^2\rangle$ (Antonia *et al.* 2000; Danaila *et al.* 1999; Danaila, Antonia & Burattini 2004), provides an analytical framework to compare between the decay characteristics of the velocity and the scalar fields.

However, the published data have not provided unambiguous support for (1.10) that is consistent with the departures, albeit small, of the decay exponent for $\langle u^2\rangle$ from $-6/5$ nor have the data provided clear support for (1.22) and (1.24). Nonetheless, from their fixed-point analysis on the transport equations for $\langle\theta^2\rangle$ and $\langle\chi\rangle$, Gonzalez & Fall (1998) found that, in the asymptotic case of large Reynolds and Péclet numbers, $\langle\theta^2\rangle \sim (x - x_0)^{-1/R}$, where

$$R = \frac{\langle\theta^2\rangle/\langle\chi\rangle}{\langle q^2\rangle/\langle\epsilon\rangle} \tag{1.25}$$

is the scalar-velocity timescale ratio, and the invariant (Gonzalez & Fall 1998)

$$\langle\theta^2\rangle L^{2/R} = \text{constant} \tag{1.26}$$

is reconcilable with (1.22) if $R = 2/3$. If $\langle u^2\rangle$ and $\langle\theta^2\rangle$ are introduced in the flow in a similar manner, the timescale ratio R can be expected to be close to one so that, for complete self-preservation of the velocity and scalar fields, $\alpha_u^L = \alpha_\theta^L = 2$. The inference is that the Saffman and Corrsin invariants are only likely to hold if R_{λ_u} is finite, in contrast to the original assumptions made by Saffman and Corrsin, and for a specific set of initial conditions.

Our approach developed in the previous subsection can be easily extended to the scalar field. If $\langle\theta^2\rangle$ decays according to a power law

$$\langle\theta^2\rangle \sim (x - x_0)^{n_\theta}, \tag{1.27}$$

then λ_θ^2, like λ_u^2, varies linearly with x, namely

$$\lambda_\theta{}^2 \sim x - x_0. \tag{1.28}$$

The linearity of $\lambda_\theta{}^2$ provides a simple way to estimate x_0. Therefore, there is an immediate invariant which involves λ_θ, i.e.

$$\langle\theta^2\rangle\lambda_\theta^{\alpha_\theta^\lambda} = \text{constant}, \tag{1.29}$$

with

$$\alpha_\theta^\lambda = -2n_\theta. \tag{1.30}$$

The normalized scalar dissipation rate is defined as

$$C_\chi = \frac{\langle\chi\rangle L_\theta}{\langle\theta^2\rangle\langle u^2\rangle^{1/2}}. \tag{1.31}$$

Provided that C_χ is constant, we obtain

$$\frac{\langle u^2\rangle^{1/2}(x - x_0)}{L_\theta} \sim \text{constant}. \tag{1.32}$$

It follows that L_θ, like L, also varies according to

$$L_\theta \sim (x - x_0)^{1+n_u/2} \tag{1.33}$$

and so, for $\langle\theta^2\rangle L_\theta{}^{\alpha_\theta^L}$ to remain constant,

$$\alpha_\theta^L = -\frac{2n_\theta}{2 + n_u}. \tag{1.34}$$

One therefore expects α_θ^L to be identical to α_u^L when n_θ and n_u are equal.

The road-map of the paper is as follows. The addressed question concerns the validity of Saffman and Corrsin invariants in passive grid turbulence. For that, we appraise the validity of (1.10) and (1.22) using new grid-turbulence data for u and θ as well as previously published data (e.g. Antonia *et al.* 2003, 2004; Lavoie *et al.* 2007) for all three components of the velocity fluctuation (u, v and w) and θ. More exactly, we explore the possibility that the relations

$$\langle u^2\rangle\lambda_u{}^{\alpha_u^\lambda} = \text{constant}, \quad \langle\theta^2\rangle\lambda_\theta{}^{\alpha_\theta^\lambda} = \text{constant}, \tag{1.35}$$

as well as their counterparts involving the integral scales L and L_θ

$$\langle u^2\rangle L^{\alpha_u^L} = \text{constant}, \quad \langle\theta^2\rangle L_\theta{}^{\alpha_\theta^L} = \text{constant} \tag{1.36}$$

are tenable with the exponents $\alpha_u^L \neq 3$ and $\alpha_\theta^L \neq 3$ without invoking the invariant assumptions (1.8) and (1.20).

The experimental details for the new measurements are given in § 2. The most stringent assumptions that are needed to relate α_u^λ and α_u^L to n_u (as well as their counterparts for the scalar) are assessed in § 3. These assumptions are: global isotropy (§ 3.1) as well as the constancy of the dimensionless dissipation rates, C_ϵ and C_χ w.r.t.

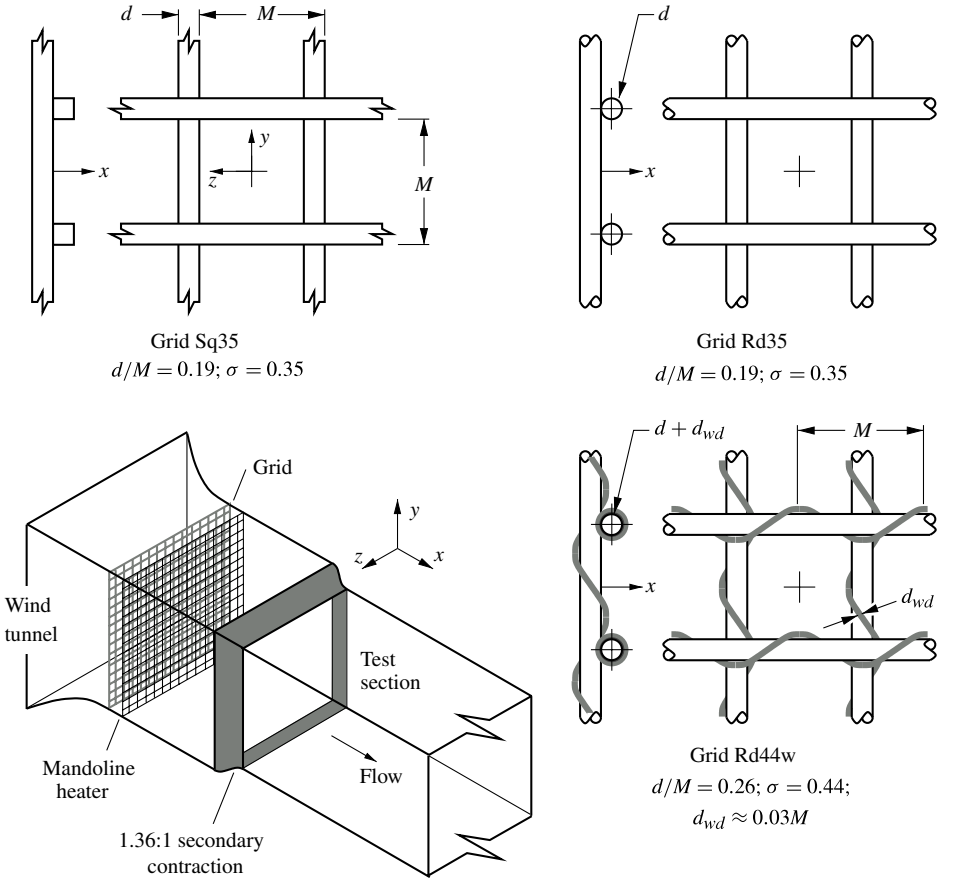

FIGURE 1. The wind-tunnel test section installed with the biplanar grid (mesh solidity is $\sigma = d/M(2 - d/M)$) and the 1.36:1 secondary contraction.

the location x (§ 3.2). In § 4, we present the results for the exponents α_u^λ, α_u^L and their counterparts for the scalar field. In § 5, the effect of increasing R_{λ_u} on the exponents are discussed in light of the available data for grid turbulence. A summary of the main findings as well as concluding remarks are given in § 6.

2. Experimental details

Figure 1 is a schematic diagram of the test section of a low-speed open-circuit wind tunnel as well as the three different biplanar grids used for the present study. A detailed description of the tunnel is given by Lavoie (2006) and Lavoie *et al.* (2007). The primary contraction has an area ratio of 9:1. The test section downstream of the secondary contraction has a nominally square cross-section of width $W \simeq 0.31$ mm (or $12M$) with an adjustable floor which allows the mean pressure gradient to be set to zero. The first grid (Sq35) is made of square bars with a solidity ratio (σ) of 0.35, the second grid (Rd35) has round bars ($\sigma = 0.35$) and the third grid (Rd44w) consists of round bars with a thin wire wrapped helicoidally around each bar ($\sigma = 0.44$). For each grid, the mesh size is $M = 24.76$ mm. In this paper, we also consider the isothermal data obtained in earlier studies for Sq35 (Antonia *et al.* 2003) and for Rd35 (Antonia,

Zhou & Zhu 1998); in the latter, all three fluctuating velocity and vorticity components were measured simultaneously. For all measurements, the mean velocity U_0 upstream of the grid is $\simeq$6 m s^{-1}, corresponding to a value of R_M ($=U_0M/\nu$) of $\simeq 10^4$.

To introduce the scalar, the grid flow is heated with a mesh of 0.5 mm diameter Chromel-A wires placed at $1.5M$ downstream of the grid (figure 1). The method of heating is based on the 'mandoline' technique (Warhaft & Lumley 1978). The horizontal and vertical wires of the mandoline heater are separated by a gap of $0.6M$ and have the same mesh size as the grids. The temperature is controlled by a variable-voltage (0–275 V) power supply. For the temperature to be passive, the grid flow is just slightly warmer than the ambient air; the temperature difference, ΔT, is $\simeq 2$°C. The Prandtl number, $Pr = \nu/\kappa$, is $\simeq 0.7$; κ is the thermal diffusivity.

To improve the isotropy of the large scales, the test section includes a (1.36:1) secondary contraction located at a distance of $11M$ downstream of the grid (figure 1). The design of the contraction is based on a linear theory (Batchelor 1953; Uberoi 1956) and empirical data (Comte-Bellot & Corrsin 1966). With the contraction, the velocity in the test section is not constant (Lee *et al.* 2012*a*,*b*) and the time for turbulence to be convected from the grid (at position $s = 0$) to a downstream location ($s = x$) is defined as (Comte-Bellot & Corrsin 1966; Lavoie *et al.* 2007)

$$t = \int_0^x \frac{1}{U(s)}\,\mathrm{d}s. \tag{2.1}$$

The non-dimensional timescale, tU_0/M (U_0 is the constant local velocity immediately upstream of the grid), allows direct comparison between results obtained downstream of the contraction and those obtained with no contraction (Lee *et al.* 2012*a*). In the absence of a contraction, equation (2.1) simplifies to $tU_0 = x$. Improvements to the large-scale isotropy for the three grids considered here are reported by Lavoie (2006) and Lavoie *et al.* (2007).

The temperature field produced by the mandoline heater approximately satisfies homogeneity, where the mean-square temperature derivatives, $\langle(\partial\theta/\partial x)^2\rangle = \langle(\partial\theta/\partial y)^2\rangle = \langle(\partial\theta/\partial z)^2\rangle$, have been verified by Danaila *et al.* (2000). The departure from $\langle(\partial\theta/\partial x)^2\rangle = \langle(\partial\theta/\partial y)^2\rangle = \langle(\partial\theta/\partial z)^2\rangle$ is significant only when a mean temperature gradient is present, e.g. using an array of wire ribbons located upstream in the plenum, known as a 'toaster' (Mydlarski & Warhaft 1998). For the most part, the level of (local) isotropy of the temperature derivatives is tested by examining the skewness and kurtosis of the temperature derivatives (Danaila *et al.* 2000; Zhou *et al.* 2003), i.e. $S_\alpha = \langle\alpha^3\rangle/\alpha'^3$ and $K_\alpha = (\langle\alpha^4\rangle/\alpha'^4) - 3$, where $\alpha = \partial\theta/\partial x$ and the prime denotes the r.m.s. value. For turbulence which is Gaussian and isotropic, both skewness (S_α) and kurtosis (K_α) is expected to be equal to zero. For the present measurements, the skewness falls in the range $-0.04 \lesssim S_\alpha \lesssim -0.10$ and is independent of streamwise distance from the grid for $22 \lesssim x/M \lesssim 110$; the kurtosis falls in the range $0.8 \lesssim K_\alpha \lesssim 1.6$ (Lee *et al.* 2012*a*).

The streamwise velocity (u) and the temperature (θ) fluctuations are measured simultaneously using hot and cold (Wollaston Pt-10 %Rh) wires. The hot wire (diameter $d_{hot} \simeq 2.50$ μm; length $l_{hot} \simeq 200d_{hot}$) is operated at constant temperature with an overheat ratio of 1.5. To minimize contamination by velocity, the cold wire ($d_{cold} \simeq 0.63$ μm; $l_{cold} \simeq 1000d_{cold}$) is operated at a constant current of 0.1 mA (the sensitivity is 1 Ω/°C). The length-to-diameter ratios of the hot/cold wires are sufficiently large to minimize end conduction losses. To avoid interference of the measurement signals, the wires are parallel with a spanwise separation of 1 mm and the cold wire is placed just upstream of the hot wire. The distance between the wires

is 1.5–3.0 Kolmogorov lengths ($\eta = \nu^{3/4}/\langle\epsilon\rangle^{1/4}$); the lengths of the wires, from the measurement position nearest to the grid to the position furthest from the grid, are $0.6 \lesssim \eta/l_{hot} < 1.5$ and $0.5 < \eta/l_{cold} \lesssim 1.1$. The signals from the hot/cold wires are digitized with a 12 bit analogue-to-digital (A/D) converter and sampled at twice the cut-off frequency of the low-pass filter. The cutoff frequency is determined by the response time of the cold wire (Antonia, Browne & Chambers 1981); it is close to but usually smaller than the Kolmogorov frequency, i.e. $0.8 \lesssim f_K(2\pi\eta/U_0) < 1$. Note that the cutoff frequency of the hot wire as determined by the square-wave test is higher than that of the cold wire.

For each experimental run, the total record duration is $\sim 10^6/f_s$, where f_s is the sampling frequency. Based on twice the integral timescale, the number of independent samples, $(10^6/f_s)/(2L_u/U_0)$, is $\sim 2 \times 10^4$–3×10^4. To ensure that the records are of sufficient duration, we have verified that the integrands associated with $\langle u^2\rangle$, $\langle\theta^2\rangle$, $\langle\epsilon\rangle$ and $\langle\chi\rangle$ have converged. For each grid, a total of nine points (for $\langle u^2\rangle$ and $\langle\theta^2\rangle$) are measured in the range $22 \lesssim x/M \lesssim 110$. Each data point for the mean dissipation rates ($\langle\epsilon\rangle$ and $\langle\chi\rangle$) is calculated by using the three-point centre-difference scheme; the outer point on each end of a batch of nine data points is calculated by extrapolating a power-law curve fit to the data points for $\langle u^2\rangle$ and $\langle\theta^2\rangle$. This avoids potential bias estimates of $\langle\epsilon\rangle$ and $\langle\chi\rangle$ as well as the need to drop measurement points using either forward or backward–difference schemes.

To summarize, the length-to-diameter (l/d) ratios of the wires are selected to minimize attenuation at high frequencies while maintaining η/l as close to one as practicable. For $\eta/l \gtrsim 0.5$, the effect of attenuation underestimates $\langle u^2\rangle$ by no more than ±2–4 % (Wyngaard 1968). For a cold wire of $l/d \simeq 1000$, the error in measuring $\langle\theta^2\rangle$ is ±5 % (Browne & Antonia 1987). The uncertainty in $\langle\epsilon\rangle$ and $\langle\chi\rangle$, estimated by method of propagation of errors (Moffat 1988), is no more than ±10 %.

3. Assessment of flow characteristics

Prior to determining of the magnitudes of the exponents α_u^L, α_u^λ (and their counterparts for the temperature field), we present in § 3.1 experimental estimates of some of the quantities involved in the analytical approach described in § 1. Particular attention is paid to the assessment of global isotropy, a basic assumption of the theory. No attention is paid to the isotropy of the small scales since it appears to be reasonably well satisfied, regardless of whether a secondary contraction is used (e.g. Antonia *et al.* 2010). The behaviour of the normalized velocity and scalar dissipation rates is assessed in more detail in § 3.2.

3.1. *Basic flow characteristics*

We first indicate the basic characteristics of the flow (variances of u and θ, as well as length scales such as λ_u, λ_θ, L and L_θ).

Figures 2 and 3 depict $\langle u^2\rangle$ and $\langle\theta^2\rangle$ as functions of $(x - x_0)/M$, respectively. For convenience, $(t - t_0)U_0$ is replaced by $(x - x_0)$ in figures 2 and 3 and all subsequent figures which present results obtained with the use of the contraction; it should be kept in mind however that, with the contraction, x no longer represents the physical distance downstream of the grid. The virtual origin is determined via the Taylor/Corrsin microscale method (Antonia *et al.* 2004; Lee *et al.* 2012*a*,*b*), i.e. by plotting $\lambda_u^2/(x - x_0)$ and $\lambda_\theta^2/(x - x_0)$ versus x for different choices of x_0, the optimum choices yielding the most convincing plateaux for these ratios. For each grid, the same

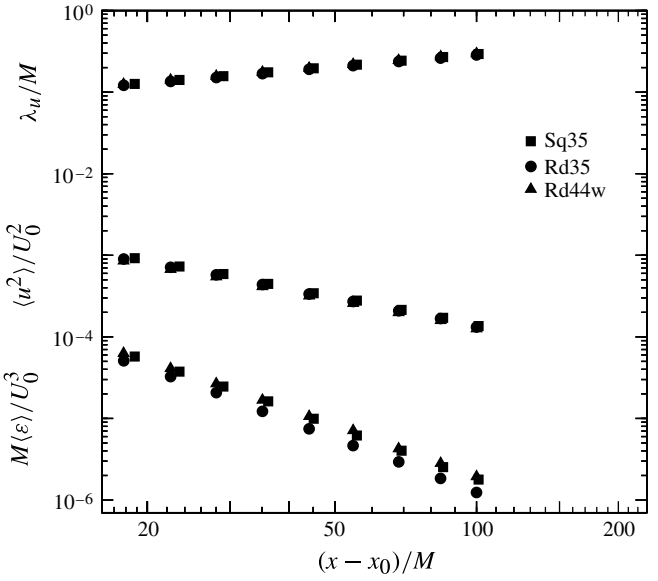

FIGURE 2. Velocity variance, mean energy dissipation rate and the Taylor microscale for different grids with the contraction. Here $R_M \simeq 10^4$.

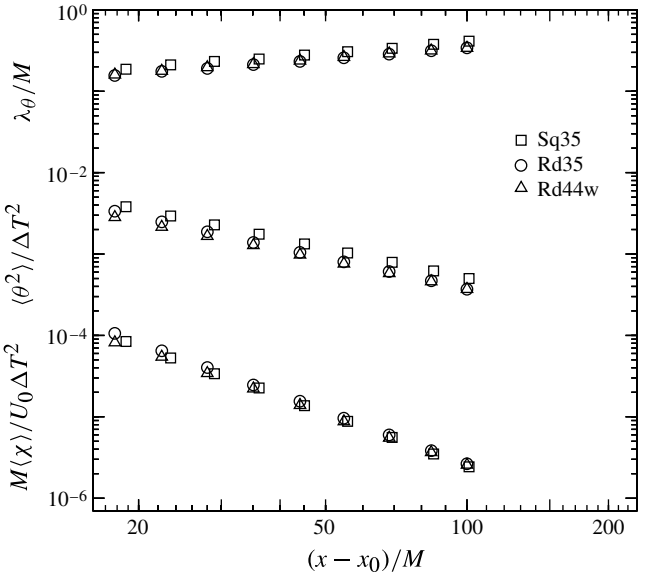

FIGURE 3. Temperature variance, mean temperature dissipation rate and the Corrsin microscale for different grids with the contraction. Here $R_M \simeq 10^4$.

optimum value of x_0/M satisfies both $\langle u^2\rangle$ and $\langle\theta^2\rangle$; changing x_0/M by ± 1.0 alters n_u and n_θ by no more than ± 0.03.

For the present grids with the contraction, Lavoie *et al.* (2007) established that the turbulence is very nearly globally isotropic ($r_{uw} = \langle u^2\rangle/\langle w^2\rangle \simeq 1$) and that

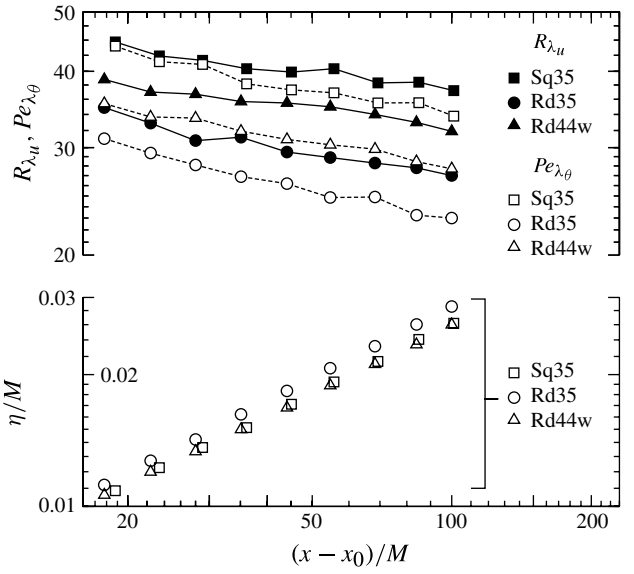

FIGURE 4. Taylor microscale Reynolds number (R_{λ_u}), Péclet number (Pe_{λ_θ}) and Kolmogorov microscale (η) for different grids with the contraction. Here $R_M \simeq 10^4$.

both $\langle q^2 \rangle \sim (x - x_0)^{n_q}$ and $\langle u^2 \rangle \sim (x - x_0)^{n_u}$ have similar rates of decay, i.e. $n_q \simeq n_u$. We have assumed axial symmetry ($\langle v^2 \rangle = \langle w^2 \rangle$) to estimate $\langle q^2 \rangle$, i.e.

$$\langle q^2 \rangle = \langle u^2 \rangle + 2\langle w^2 \rangle = [1 + (2/r_{uw})]\,\langle u^2 \rangle \tag{3.1}$$

using the present measurements of $\langle u^2 \rangle$.

For grid turbulence, the turbulent energy budget is approximated by (1.5), see Zhou *et al.* (2000), and the Taylor microscale is given by

$$\lambda_q{}^2 = 5\nu\langle q^2 \rangle / \langle \epsilon \rangle. \tag{3.2}$$

For isotropy at both large and small scales, i.e. $\langle q^2 \rangle = 3\langle u^2 \rangle$ and $\langle \epsilon \rangle = 15\nu\langle (\partial u/\partial x)^2 \rangle$, respectively, relation (3.2) reduces to the more common definition of the longitudinal Taylor microscale, namely $\lambda_q = \lambda_u$ or $\lambda_u{}^2 \equiv \langle u^2 \rangle / \langle (\partial u/\partial x)^2 \rangle$, see Monin & Yaglom (1975). Under these conditions, the Taylor microscale Reynolds number $R_{\lambda_q} = (\langle q^2 \rangle/3)^{1/2}\lambda_q/\nu$ reduces to the more usual definition $R_{\lambda_u} = \langle u^2 \rangle^{1/2}\lambda_u/\nu$. Although only R_{λ_u} is plotted in figure 4, its magnitude differs from that of R_{λ_q} by no more than 10 %.

For the passive scalar, the Corrsin microscale is given by

$$\lambda_\theta{}^2 = 6\kappa\langle \theta^2 \rangle / \langle \chi \rangle. \tag{3.3}$$

For $\langle \chi \rangle = 3\kappa\langle (\partial\theta/\partial x)^2 \rangle$ (assuming isotropy at small scales), equation (3.3) can be identified with the more common definition $\lambda_\theta{}^2 = 2\langle \theta^2 \rangle / \langle (\partial\theta/\partial x)^2 \rangle$, see Monin & Yaglom (1975, p. 145).

Included in figures 2 and 3 are the dissipation rates of the kinetic energy and of the scalar variance, as well as the scales λ_u and λ_θ. There is only a small effect of grid geometry on these quantities. In particular, the decay rate of $\langle \epsilon \rangle$ is larger for Rd35 than for the other two grids, reflecting the larger magnitude of n_u for this grid. Also, the decay rate for $\langle \chi \rangle$ is slightly larger for Rd35 than for the other two grids,

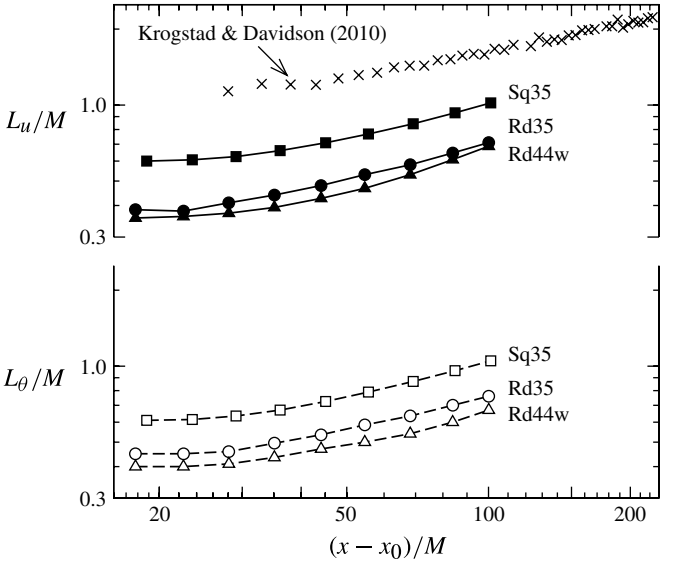

FIGURE 5. Integral length scales (L_u and L_θ) for different grids. For clarity, the L_u data ($\times$) of Krogstad & Davidson (2010) are vertically offset by a factor of two.

reflecting a slight difference in the magnitude of n_θ between the three grids (refer to § 4).

Figure 4 shows the effect of grid geometry on the Taylor microscale Reynolds number R_{λ_u} and the Corrsin microscale Péclet number

$$Pe_{\lambda_\theta} = \frac{\lambda_\theta}{\kappa}\left(\frac{\langle q^2\rangle}{3}\right)^{1/2}. \tag{3.4}$$

For all of the measurements, the grid-mesh Reynolds number $R_M = MU_0/\nu$ is constant ($\simeq 10^4$). Although η is only slightly affected by the initial conditions, the magnitudes of R_{λ_q} and Pe_{λ_θ} appear to be more affected than η (represented in figure 4). For each grid, $\langle u^2\rangle$ (or $\langle\theta^2\rangle$) and $\langle\epsilon\rangle$ (or $\langle\chi\rangle$) undergo changes and the resulting values of R_{λ_q} and Pe_{λ_θ} also change.

Figure 5 displays the integral length scale associated with the correlation function $B_{\psi\psi}$ (for $\psi \equiv u$ or θ), namely

$$B_{\psi\psi}(r) = \langle\psi(x)\psi(x+r)\rangle, \quad L_\psi = \int_0^{r_\psi} \frac{B_{\psi\psi}(r)}{\langle\psi^2\rangle}\,\mathrm{d}r, \tag{3.5}$$

where r_ψ is the separation corresponding to the first zero crossing of $B_{\psi\psi}(r)$. Figure 5 shows that, for $(x - x_0) \lesssim 30M$, the trends exhibit a slight curvature that is reminiscent of that noted in the literature (Krogstad & Davidson 2010, 2011; Valente & Vassilicos 2012). The curvature is possibly due to initially developing turbulence and the acceleration due to the secondary contraction. In § 4, we show that this translates to a mild departure from constancy of relations (1.36) for $(x - x_0) \lesssim 30M$. For measurements obtained nearest to the wind-tunnel exit, the integral length scale (L_ψ) does not exceed 8 % of the width ($W \simeq 12M$) of the test section.

In this paper, we consider grid data obtained with and without a contraction. Using a contraction improves the isotropy at large scales for all of the grids, as reported by

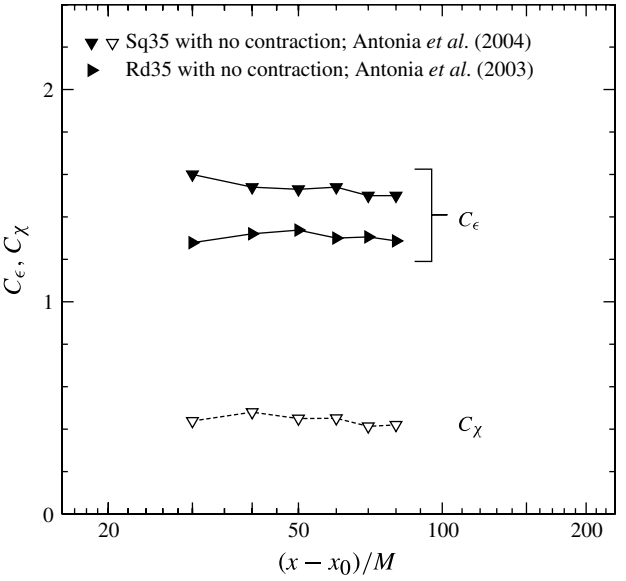

FIGURE 6. Mean energy and temperature variance dissipation-rate parameters, C_ϵ and C_χ, for grids Sq35 and Rd35; data from Antonia *et al.* (2003, 2004).

Lavoie (2006) and Lavoie *et al.* (2007). The departure from global isotropy can be as large as 15 % without the contraction. The length scales for Sq35 are larger than for the other two grids, most likely due to differences in the large-scale structures. Grid Rd44w is characterized by the smallest correlation length scales, as well as the best global isotropy (Lavoie *et al.* 2007).

3.2. *Dissipation-rate parameters*

Figure 6 shows the data of Antonia *et al.* (2004) for Sq35 with no contraction. The dissipation-rate parameters C_ϵ and C_χ are approximately independent of $(x - x_0)/M$ when the latter exceeds about 40. The magnitude of C_ϵ depends on the grid geometry; it is larger for Sq35 ($\simeq$1.24) than for Rd35 ($\simeq$1.03). For Sq35, the magnitude of C_χ ($\simeq$0.29) is smaller than that of C_ϵ by a factor slightly larger than three. From (1.3) and (1.31), the ratio C_ϵ/C_χ can be expressed as $3R(L_u/L_\theta)$ using the definition of the timescale ratio R given by (1.25). The departure of this ratio from three reflects slight departures from one of R and the length scale ratio (Zhou *et al.* 2000).

Figure 7 shows, for Sq35, the effect of the contraction on the parameters C_ϵ and C_χ. It is clear that the use of the contraction reduces the magnitude of C_ϵ by $\sim$10 %, whereas it has almost no effect of C_χ. The present data for C_ϵ and C_χ with a contraction, are shown in figure 8. Several comments can be made. First, the present values of C_ϵ are in close agreement with those obtained from the larger velocity data set of Lavoie (2006). The figure confirms that C_ϵ is affected by the grid geometry; in particular, C_ϵ is closer to one for Rd44w, for which isotropy is nearly satisfied by all of the scales. Further, it confirms that C_χ is essentially unaffected by the grid geometry. As for figure 6, the ratio of C_ϵ and C_χ in figures 7 and 8 departs from three due to small departures from one of R and L_u/L_θ (Lee *et al.* 2012*a*).

Figure 9 shows that, for Rd35, the longitudinal velocity correlation function $B_{uu}(r)/\langle u^2\rangle$ first becomes negative at $r \gtrsim 10\lambda_u$ before returning to zero, whereas for

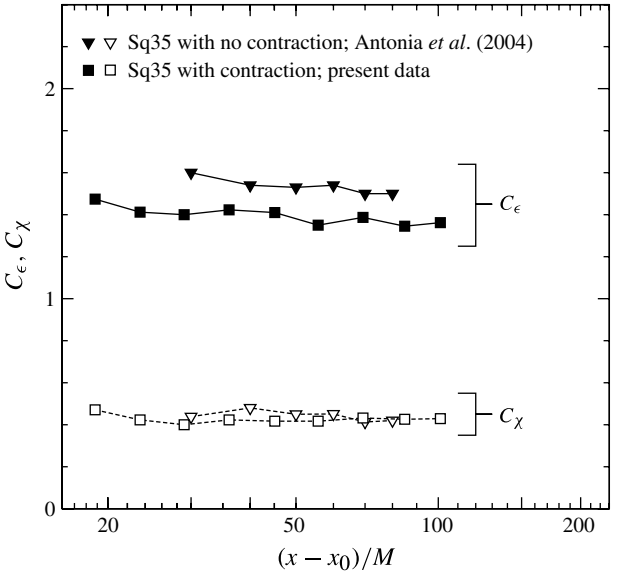

FIGURE 7. Mean energy and temperature variance dissipation-rate parameters, C_ϵ and C_χ, for grid Sq35 with and without the secondary contraction.

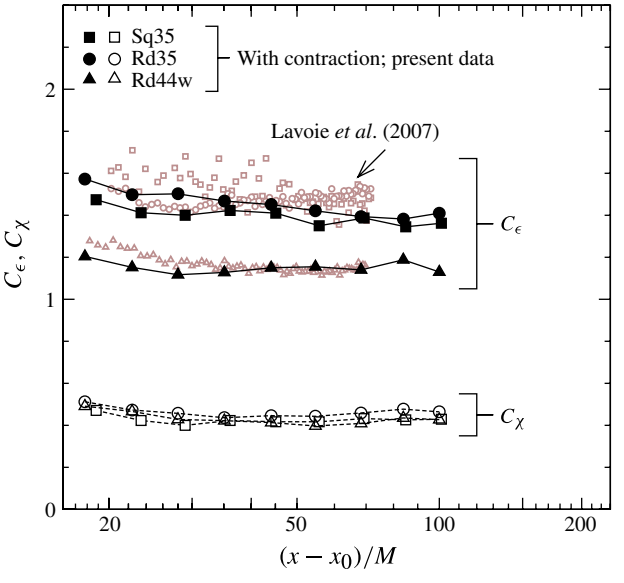

FIGURE 8. (Colour online) Dissipation-rate parameters C_ϵ and C_χ. Symbols are defined in the legend; the data of Lavoie *et al.* (2007) are shown as grey (brown online) symbols.

Sq35, it approaches zero monotonically. With the contraction, $B_{uu}(r)/\langle u^2 \rangle$ behaves in a similar manner but the 'overshoot' at $r \gtrsim 10\lambda_u$ is less evident. The overshoot suggests some form of large-scale (quasi-periodic) organization; flow visualizations (Lavoie 2006) have indicated that, for a grid constructed from circular cylinders, the

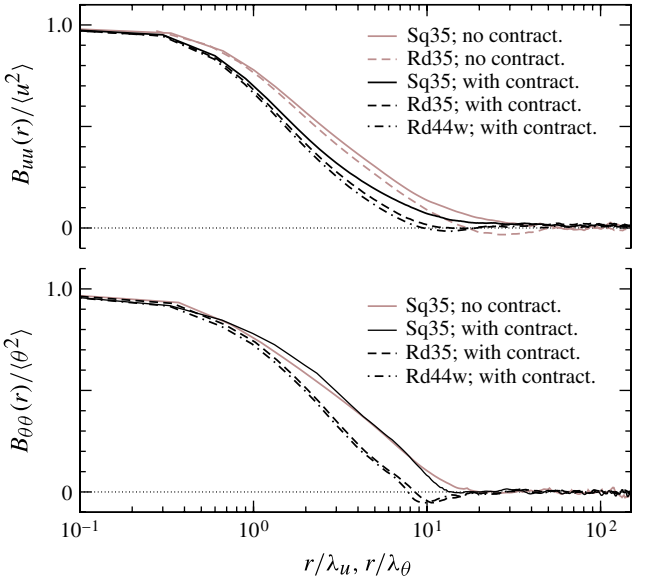

FIGURE 9. (Colour online) Correlation functions $B_{uu}(r)/\langle u^2\rangle$ and $B_{\theta\theta}(r)/\langle\theta^2\rangle$ for grids without (Antonia *et al.* 2003, 2004) and with the contraction (present data), with $x/M \simeq 80$ and $R_M \simeq 10^4$.

periodicity due to vortex shedding is discernible at larger values of x/M than for a grid of square bars. With the contraction, and also if a small diameter wire is helicoidally wrapped around the circular cylinders (i.e. grid Rd44w), the overshoot/periodicity is reduced. Unfortunately, since no measurements without the secondary contraction with this grid are available, one cannot attribute the reduction of the overshoot to either the secondary contraction and/or the wire wrapping.

In figure 9, the temperature correlation function $B_{\theta\theta}(r)/\langle\theta^2\rangle$ is obtained at the same downstream location ($80M$) as for the velocity correlation function. For Sq35, $B_{\theta\theta}(r)/\langle\theta^2\rangle$ is not visibly affected by the contraction except for a slightly steeper 'roll off' in the range $10 \lesssim r/\lambda_\theta \lesssim 20$. With the contraction, $B_{\theta\theta}(r)/\langle\theta^2\rangle$, like $B_{uu}(r)/\langle u^2\rangle$, approaches zero monotonically for Sq35; for grids Rd35 and Rd44w that produce the more periodic turbulence, there is a distinct local minimum, where the correlation is negative, at r/λ_θ (or r/λ_u) of about 10. For the present measurements, L_θ/L_u lies between 0.9 and 1.2; for the same x/M, L_θ is larger for Sq35 than for Rd35 and Rd44w.

4. Testing the invariants

The methodology adopted here is as follows. First, for each experiment, we determine the decaying exponents n_u and n_θ (e.g. see table 1 for values of n_u). Second, the values of α_u^λ and α_θ^λ are determined directly via (1.16) and (1.30), respectively. Third, the values of α_u^L and α_θ^L are determined directly via (1.19*b*) and (1.34), respectively. With these values of α_u^L, α_θ^L, α_u^λ and α_θ^λ, we check the validity of the corresponding invariants over the range of $(x - x_0)/M$ for which homogeneity and isotropy apply.

In figure 10, the parameters $(\langle u^2\rangle/{U_0}^2)(\lambda_u/M)^{\alpha_u^\lambda}$ and $(\langle\theta^2\rangle/\Delta T^2)(\lambda_\theta/M)^{\alpha_\theta^\lambda}$ are constant w.r.t. $(x - x_0)/M$, both for the present measurements and those of Lavoie

https://doi.org/10.1017/jfm.2013.217 Published online by Cambridge University Press

References	Data source	$\frac{x}{M}$	R_{λ_u}	Decay method $-n_u$	Decay method $\frac{x_0}{M}$	Microscale method $-n_u$	Microscale method $\frac{x_0}{M}$	Symbol	Description
Passive grids									
Kistler & Vrebalovich (1966)	Figure 1	20–60	670	1.04	7.0	1.01	4.5	◯	Rd33.5
Schedvin, Stegen & Gibson (1974)	Data not supplied	35–41	280	1	0	/	/	□	Sq30
Sreenivasan *et al.* (1980)	Figure 1	20–120	34	1.20	3.0	1.23	3.0	◇	Rd44
Sirivat & Warhaft (1983)	Figures 4 and 5	35–130	26.4	1.29	0	1.30	3.0	△	Sq34
		40–150	36.5	1.37	0	1.42	5.0	◁	Sq34
Makita (1991)	Figure 9	20–100	28	1.32	6.0	1.30	5.5	▽	See note[a]
Antonia *et al.* (2003)	Figure 3	30–80	40	1.26	2.0	1.25	0	⊞	Rd35
Antonia *et al.* (2004)	Figure 3	30–80	50	1.33	0	1.33	0	⊡	Sq35
Krogstad & Davidson (2010)	Figures 4 and 6	70–180	75	1.11	7.3	1.12	6.0	⊖	Sq44p
Present data	Present figure 2	22–110	40	1.18	4.5	1.18	5.0	■	Sq35
		22–110	30	1.21	5.0	1.23	6.0	•	Rd35
		22–110	35	1.13	5.5	1.14	6.0	▲	Rd44w
Active grids									
Makita (1991)	Figure 9	20–100	387	1.10	0	1.12	1.5	▷	Rotating
Mydlarski & Warhaft (1996)	Figure 3	30–70	319	1.21	0	1.24	2.0	⊕	grid bars
Kang, Chester & Meneveau (2003)	Table 1	20–48	667	1.00	0	1.08	4.0	⊠	fitted with
Larssen & Devenport (2011)[b]	Table 1; $U_0 \simeq 12$ m s^{-1}	21–48	644	1.02	3.0	1.04	3.5	⊙	agitator
	Table 1; $U_0 \simeq 15$ m s^{-1}	21–48	772	1.00	4.0	1.02	5.5	×	Wings

TABLE 1. The decay exponent (n_u) for passive and active grids. [a] Note that, for Makita (1991), the full range of the data ($x/M = 10$–100) yields $-n_u = 1.28$ with $x_0/M = 11.5$ for the passive grid (static bars with wings), and $-n_u = 1.43$ with $x_0/M = -9.2$ for the active grid (rotating bars with wings). [b] For Larssen & Devenport (2011), the values are determined from the decay of $\langle u^2 \rangle$ at five streamwise locations for two different free stream velocities, nominally 12 and 15 m s^{-1}; the rotation rate of the grid bars is 4 Hz.

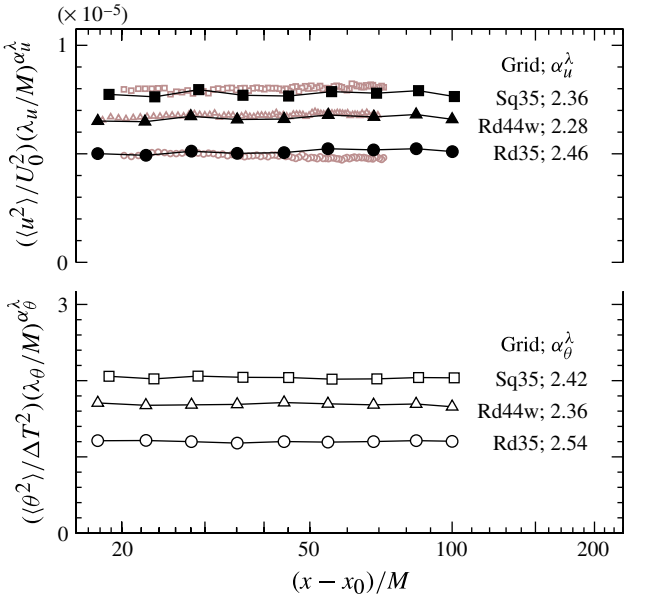

FIGURE 10. (Colour online) Plots of $(\langle u^2\rangle/U_0{}^2)(\lambda_u/M)^{\alpha_u^\lambda}$ and $(\langle\theta^2\rangle/\Delta T^2)(\lambda_\theta/M)^{\alpha_\theta^\lambda}$ for different grids with the contraction; $\alpha_u^\lambda = -2n_u$ and $\alpha_\theta^\lambda = -2n_\theta$. The present data are shown as black or white symbols. The data of Lavoie *et al.* (2007) are shown as grey (brown online) symbols with $-n_u = \alpha_u^\lambda/2 = 1.18$ (Sq35), 1.22 (Rd35) and 1.10 (Rd44w).

et al. (2007), where a large number of data points was used with small increments for $(x - x_0)/M$. The values of α_u^λ and α_θ^λ that yield plateaux are those given by (1.16) and (1.30); the different magnitudes of the plateaux reflect the dependence on the grid geometry. Figure 10 shows that, for the present velocity data, the values of $-n_u = \alpha_u^\lambda/2$ (=1.18, 1.23 and 1.14 for Sq35, Rd35 and Rd44w, respectively; see also table 1) are in close agreement with those obtained from the data of Lavoie *et al.* (2007); for the present temperature data, $-n_\theta = \alpha_\theta^\lambda/2 = 1.21$, 1.27 and 1.18 for Sq35, Rd35 and Rd44w, respectively.

As an example, the effect of changing the values of α_u^λ and α_θ^λ is shown in figure 11 for Rd44w; Sq35 and Rd35 produce similar trends. It is clear that the optimum values of α_u^λ and α_θ^λ are indeed those given by (1.16) and (1.30).

Figure 12 shows that the parameters $(\langle u^2\rangle/U_0{}^2)(L_u/M)^{\alpha_u^L}$ and $(\langle\theta^2\rangle/\Delta T^2)(L_\theta/M)^{\alpha_\theta^L}$ are constant for $(x - x_0)/M \gtrsim 30$, i.e. over the range where homogeneity should hold. The different magnitudes of the plateaux reflect the effect of grid geometry. The slight curvature exhibited by the distributions of L_u and L_θ (figure 5) for $(x - x_0)/M < 30$ can be observed in figure 12. The curvature of L_u over the region $(x - x_0)/M < 30$ is most likely due to the changes that occur to the large scales in this development region. The Taylor microscale λ_u (figure 2) does not seem to be significantly affected by these changes, as the evolution with $(x - x_0)/M < 30$ in figure 2 indicates. Consequently, the plateaux in figure 10 are more extensive than in figure 12.

For a round-bar grid of the same solidity as Rd44w and with mandoline heating of the flow downstream of this grid with no contraction, Sreenivasan *et al.* (1980) obtained the relations $\langle u^2\rangle/U_0{}^2 = 0.04(x/M - 3)^{-1.20}$, $\langle\theta^2\rangle/\Delta T^2 = 0.124(x/M - 3)^{-1.44}$, $L_u/M = 0.13(x/M - 3)^{0.4}$ and $L_\theta/L_u \simeq 0.825$. The data of Sreenivasan *et al.*

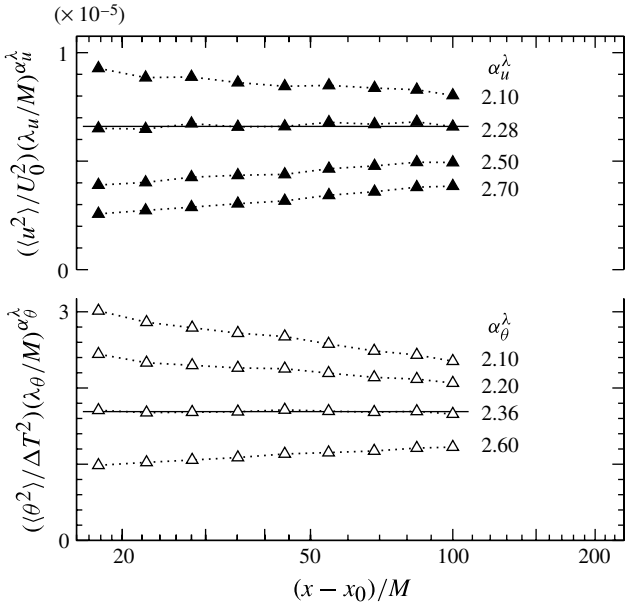

FIGURE 11. Plots of $(\langle u^2\rangle/{U_0}^2)(\lambda_q/M)^{\alpha_u^\lambda}$ and $(\langle\theta^2\rangle/\Delta T^2)(\lambda_\theta/M)^{\alpha_\theta^\lambda}$ with different values of α_u^λ and α_θ^λ for grid Rd44w with the contraction. Values that yield the plateaux (i.e. horizontal lines) are given by $\alpha_u^\lambda = -2n_u$ and $\alpha_\theta^\lambda = -2n_\theta$.

(1980) yield constant values of $C_\epsilon \simeq 1.17$ (assuming $\langle q^2\rangle = 3\langle u^2\rangle$), $C_\chi \simeq 0.39$, $(\langle u^2\rangle/{U_0}^2)(L_u/M)^{\alpha_u^L} \simeq 0.9 \times 10^{-4}$ and $(\langle\theta^2\rangle/\Delta T^2)(L_\theta/M)^{\alpha_\theta^L} \simeq 0.4 \times 10^{-4}$ which are not too different from the present measurements for Rd35 and Rd44w (figure 12).

Krogstad & Davidson (2010, figure 10) noted that C_ϵ decreased slightly with increasing x/M. Valente & Vassilicos (2012) suggested that there are non-negligible effects due to inhomogeneity in the region $((x - x_0)/M < 70)$ and (electronic) noise when $(x - x_0)/M > 180$. A statistical hypothesis test of Krogstad & Davidson's (2010, figures 10 and 11) data shows that, at a 99 % level of confidence, C_ϵ and $(\langle u^2\rangle/{U_0}^2)(L_u/M)^{\alpha_u^L}$ are independent of $(x - x_0)/M$ for $70 \lesssim (x - x_0)/M \lesssim 180$.

From figures 10 and 12, it is clear that there is an advantage in opting for (1.35) rather than (1.36) since the Taylor microscale can be determined more reliably than the integral length scale L_u provided that reliable estimates of $\langle\epsilon\rangle$ and $\langle\chi\rangle$ can be made. The former scale requires knowledge of $\langle u^2\rangle$, $\langle\theta^2\rangle$, $\langle\epsilon\rangle$ and $\langle\chi\rangle$; for the majority of passive grid experiments, the mean dissipation rates are readily available via (1.5) and (1.23). In estimating L_u, there is inevitable arbitrariness when integrating the velocity correlation function $B_{uu}(r)$ up to its first zero crossing. While the exponents α_u^L and α_θ^L are given by (1.19*b*) and (1.34), the exponents α_u^λ and α_θ^λ are simply proportional to n_u and n_θ, as expressed by (1.16) and (1.30).

5. Effect of the Reynolds number on n_u

The issue of how n_u behaves as R_{λ_u} increases deserves some attention. Mohamed & LaRue (1990) examined a wide range of passive grid data and found that $-n_u$ ($\simeq$1.30) was approximately constant over a factor of 10 variation in R_M (the maximum R_{λ_u} was about 100). George (1992*b*, figure 2) plotted the variation of $-n_u$ with R_M for

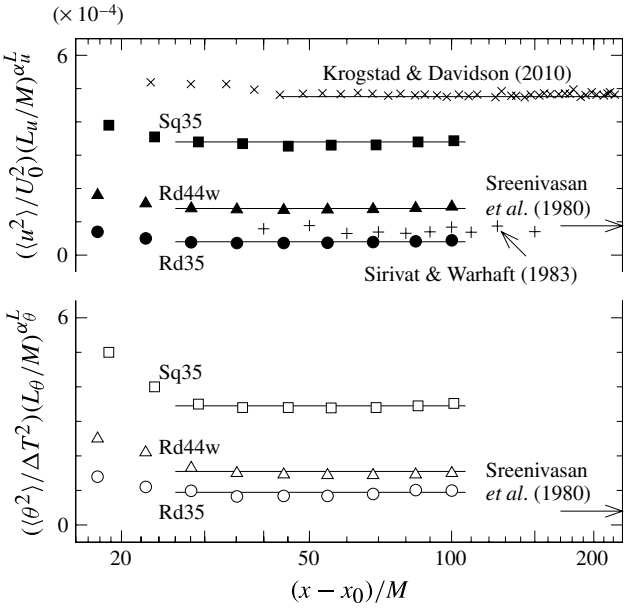

FIGURE 12. Plots of $(\langle u^2\rangle/{U_0}^2)(L_u/M)^{\alpha_u^L}$ and $(\langle\theta^2\rangle/\Delta T^2)(L_\theta/M)^{\alpha_\theta^L}$ for different grids; the present data are shown as black and white symbols; α_u^L and α_θ^L are given by (1.19*b*) and (1.34), respectively. The data of Sirivat & Warhaft (1983) ($+R_{\lambda_u} \simeq 36.5$) and Krogstad & Davidson (2010) ($\times R_{\lambda_u} \simeq 75$) are vertically offset by 0 and 4×10^{-4}, respectively.

the square-bar grid data of Comte-Bellot & Corrsin (1966) and Kistler & Vrebalovich (1966) (maximum $R_{\lambda_u} = 670$) and concluded that the trend of $-n_u$ is clearly downward as R_M increases. Although the dependence of $-n_u$ on the grid geometry cannot be dismissed, it would appear that R_M has the major effect on $-n_u$. George & Davidson (2004) pointed out that there is no evidence that the turbulence evolves toward the final period of decay for which $-n_u = 5/2$. This latter behaviour has been observed only when R_M is sufficiently small (Bennett & Corrsin 1978). In figure 13, values of $-n_u$ are plotted against R_{λ_u} for all of the passive grid data listed in table 1. The plot suggests that $-n_u$ approaches one when R_{λ_u} exceeds ~500, although it is evident that more passive grid data points in the range $100 \lesssim R_{\lambda_u} \lesssim 1000$ (only the measurements of Kistler & Vrebalovich (1966) and Schedvin *et al.* (1974) fall in this range) are needed to confirm this trend.

Active grid turbulence experiments (such as those of Makita (1991), Mydlarski & Warhaft (1996), Kang *et al.* (2003) and Larssen & Devenport (2011, referred to hereafter as LD11)) have yielded quite a large number of data in this range. The main tendency has been to provide statistics at one location in the flow and only a few estimates of n_u have been inferred from the spatial decay rate of $\langle u^2\rangle$; correspondingly few estimates of $\langle\epsilon\rangle$ have been made via relation (1.5). Table 1 shows that, apart from Makita (1991), the range of x/M used for these estimates is smaller than that used in passive grid experiments. In figure 13, we have collated values of n_u for these experiments; all of the grid designs are essentially based on that of Makita (1991), which uses rotating grid bars equipped with agitator wings. The integral length scale of the resulting turbulence is generally larger than for conventional passive grids. For all of the data in table 1, we have obtained our estimates of n_u from the decay rate of

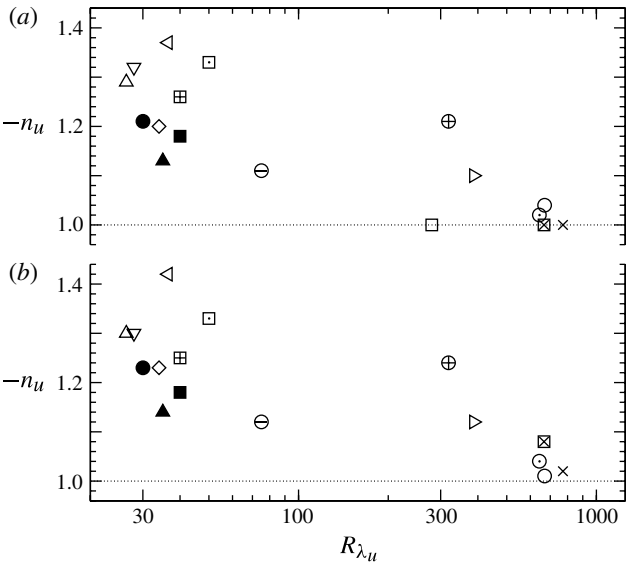

FIGURE 13. The decay exponent (n_u) as a function of R_{λ_u}; (a) the decay method $\langle u^2\rangle \sim (x - x_0)^{n_u}$ and (b) the microscale method (5.1) are used. Table 1 defines the symbols.

$\langle u^2\rangle \sim (x - x_0)^{n_u}$, where the choice of x_0 ensures that n_u is constant in the power-law decay range; the approach is the same as that described by Mohamed & LaRue (1990), Lavoie *et al.* (2007) and Lee *et al.* (2012*a*); the values of n_u obtained from this 'decay' method are shown in figure 13(*a*).

Makita (1991) estimates of n_u ($10 \lesssim x/M \lesssim 100$) are associated with rather large magnitudes of the virtual origin, i.e. $-n_u = 1.28$ with $x_0/M = 11.5$ for the passive grid, and $-n_u = 1.43$ with $x_0/M = -9.2$ for the active grid. This is most likely due to flow inhomogeneity (the flow is still developing and anisotropic) in the range $x/M < 20$ since the data of Makita (1991, figure 9) deviate considerably from the power-law decay in this range. To circumvent this problem, we have discounted Makita's data points at $x/M < 20$ when estimating n_u. In table 1, all estimates are obtained by using data points at $x/M \gtrsim 20$ (this range ensures that the flow is reasonably homogeneous while retaining most of the data points to allow a satisfactory curve fit); the 95 % confidence limit for the estimated values of n_u is about ± 0.05. For nearly all experiments using a passive grid (Kistler & Vrebalovich 1966; Sreenivasan *et al.* 1980; Sirivat & Warhaft 1983; Antonia *et al.* 2003, 2004; Krogstad & Davidson 2010) and one with an active grid (Mydlarski & Warhaft 1996), the values of n_u are very close to those reported by these authors; the difference is no more than ± 0.04.

Figure 13(*a*) and table 1 show that, for the experiments at high R_{λ_u} of about 600–800 (Kistler & Vrebalovich 1966; Kang *et al.* 2003; LD11), the value of $-n_u$ obtained from the decay method is 1.0. For the Kistler & Vrebalovich (1966) data point (labelled ◯), we estimated n_u using all of the $\langle u^2\rangle$ data from their figure 1. For Kang *et al.* (2003) (⊠), we used the values of $\langle u^2\rangle$ from their table 1 to estimate n_u, although they quoted a larger decay exponent of 1.25 from their power-law curve fit of $\langle q^2\rangle = \int_0^{\pi/\Delta} E(k)\,\mathrm{d}k$ using different filter scales Δ (figure 7 of their paper). For LD11, we have estimated n_u from their table 1 at five streamwise locations for two different free stream velocities, nominally 12 and 15 m s^{-1}. In each case, R_M is

constant ($\simeq 1.7 \times 10^5$ and 2.1×10^5) as are all other parameters associated with the operational protocol for the rotating elements of the grid. The value of n_u, inferred from the decay rates of $\langle u^2 \rangle$, is 1.02 (labelled $\odot$) and 1.00 ($\times$) for the respective R_M values. Surprisingly, Schedvin *et al.* (1974) obtained $-n_u = 1$ ($\square$) despite the uncertainty associated with the rather narrow range of x/M (= 35, 38, 40 and 41). Due to this narrow range, Schedvin *et al.* (1974) indicated that a range of values (e.g. $-n_u = 1.00$ and 1.25; $x_0/M = 0$, 2 and 4) can give equally satisfactory fits to the data.

However, the data points for $\langle u^2 \rangle$ are not given in Schedvin *et al.* (1974)'s paper, we have not been able to check their values of n_u.

As a consistency check, estimates of $-n_u$ for the passive and active grid data have also been made using the relation (also known as the 'Taylor microscale' method),

$$-n_u = \frac{10\nu}{\lambda_u^2}\frac{(x-x_0)}{U_0} \equiv \frac{2}{1+(2/r_{uw})}\frac{\langle \epsilon \rangle}{\langle u^2 \rangle}\frac{(x-x_0)}{U_0}, \tag{5.1}$$

derived from (1.5) and (3.1). The results obtained from (5.1) are presented in figure 13(*b*) and table 1. Where the value of r_{uw} is not provided by the authors, we assumed it is one, an assumption that is strictly justifiable only for isotropic grid turbulence. This assumption seems acceptable for LD11 who measured values of r_{uw} quite close to one, because of the placement of the grid in the wind-tunnel contraction. The choice of x_0 ensures that $\lambda_u^2/(x-x_0) \sim (-\nu/n_u)$ is constant in the power-law decay range ($x \gtrsim 20M$), where the flow is expected to be sufficiently homogeneous. Note that the uncertainty in measuring $\langle \epsilon \rangle$ is a source of error in estimating $-n_u$ from (5.1). For a fixed value of x_0, varying $\langle \epsilon \rangle$ by $\pm 20\,\%$ changes n_u by no more than ± 0.2. With the exception of LD11, the values of $\langle \epsilon \rangle$ reported by the authors have led to values of $-n_u$ which are in general agreement with those inferred from the decay method; the difference is no more than ± 0.08.

For the LD11 data, we have focused on only two cases ($U_0 \simeq 12$ and 15 m s^{-1}) where the measurements of $\langle u^2 \rangle$ are made at $x/M = 21.3$, 29.3, 37.3, 41.0 and 47.5. For these two cases, we only used our estimates of $\langle \epsilon \rangle$ from (1.5) to determine n_u with (5.1). This is prompted by Larssen & Devenport (2002)'s comment that their estimates of $\langle \epsilon \rangle$ are in error by at least 20 % (this error increases with distance upstream) and therefore unreliable because the low-frequency end of the spectrum shows the greatest departure from the 'standard homogeneous isotropic form'. In fact, using LD11's measurements of $\langle u^2 \rangle$, our estimates of $\langle \epsilon \rangle$ differ from their estimates by 33–45 % for the furthest three (x/M) locations and by 81–110 % for the closest two locations (this is checked using forward and backward difference schemes). LD11 noted that the lowest wavenumbers are attenuated due to the limited size of the test section (their table 1 indicates that the integral length scale is essentially constant with x) whilst the major injection of energy by the grid is at the start of the inertial range. Be that as it may, it is difficult to dismiss the possibility that the dissipative end of the spectrum is attenuated due to the finite lengths of the hot wires. Larssen & Devenport (2002)'s observation that estimates of $\langle \epsilon \rangle_{iso}$ as obtained from single hot wires with lengths equal to 1.7 mm and 0.5 mm (η is about 0.2 mm at $R_{\lambda_u} \simeq 800$) differ by only 9 % is not easily reconcilable with Wyngaard (1969) results for the effect of l_w/η on $\langle (\partial u/\partial x)^2 \rangle$. As most of the LD11 data on $\langle u^2 \rangle$ (at different U_0) are provided at only one x/M location in the grid flow, it is difficult to have confidence in the estimates of n_u with (5.1) because of the large combined uncertainties in $\langle \epsilon \rangle$

and x_0. For example, for the LD11 case with the largest R_{λ_u} ($= 1362$; $x/M = 21.3$; $U_0 \simeq 20$ m s^{-1}), using (5.1) with $r_{uw} = 1$, $x_0 = 0$ and their values for $\langle u^2 \rangle$ and $\langle \epsilon \rangle$ yields a value of $-n_u$ ($\simeq 0.4$) which is significantly smaller than one. To summarize, equation (5.1) is useful provided that $\langle u^2 \rangle$ is available for a sufficient range of x/M; this is so that $\langle \epsilon \rangle$ can be satisfactory estimated/checked via (1.5) before choosing x_0 to ensure that the value of n_u is constant in the power-law decay range.

Notwithstanding the scatter, figure 13 shows that, for both methods of estimating n_u, the overall trend of $-n_u$ is downward as R_{λ_u} increases, which is consistent with George (1992*b*)'s observation. Both active and passive grid data seem to imply that a value of $-n_u$ close to one could be reached when R_{λ_u} is ~ 1000.

6. Conclusions and discussion

The present study of the initial period of decay for passive grid turbulence at relatively small values of the grid-mesh Reynolds number, R_M, allow three major conclusions to be drawn.

(1) First, the measured products $\langle u^2 \rangle {\lambda_u}^{\alpha_u^\lambda}$ and $\langle \theta^2 \rangle {\lambda_\theta}^{\alpha_\theta^\lambda}$, with $\alpha_u^\lambda = -2n_u$ and $\alpha_\theta^\lambda = -2n_\theta$ are independent of x. This seems to highlight the importance of the Taylor and Corrsin microscales in the context of determining the invariants for this flow. We recall that earlier work (Antonia *et al.* 2003; Antonia & Orlandi 2004) confirmed the adequate similarity of the transport equations for the second-order velocity and temperature structure functions with λ_u and λ_θ as the relevant length scales. The invariance w.r.t. x of $\langle u^2 \rangle {\lambda_u}^{-2n_u}$ and $\langle \theta^2 \rangle {\lambda_\theta}^{-2n_\theta}$ can certainly be tested with confidence since there is no ambiguity in determining λ_u and λ_θ.

(2) The values of the exponents α_u^L and α_θ^L required for $\langle u^2 \rangle {L_u}^{\alpha_u^L}$ and $\langle \theta^2 \rangle {L_\theta}^{\alpha_\theta^L}$ to remain constant with x are given by relations (1.19*b*) and (1.34) provided that the non-dimensional dissipation rate parameters C_ϵ and C_χ do not vary with x. This constancy is adequately supported by all of the data examined in this paper. There is however some uncertainty associated with the constancy w.r.t. x of $\langle u^2 \rangle {L_u}^{\alpha_u^L}$ and $\langle \theta^2 \rangle {L_\theta}^{\alpha_\theta^L}$ due mainly to the ambiguity in determining the integral length scales. The departures of α_u^L and α_θ^L from the value of 3 which essentially correspond to the deviations of α_u^λ and α_θ^λ from the value of 2.4, underline that the Saffman and Corrsin invariants are not strictly satisfied by the data. These departures reflect mainly the dependence of n_u and n_θ on the initial conditions, i.e. the particular type of grid that is used and, more likely, the magnitude of R_M.

(3) The magnitude of C_ϵ appears to be more sensitive to the grid geometry than that of C_χ. The latter is essentially the same for the three grids that have been used, possibly due to the use of the same initial heating conditions. Also, the effect of the secondary contraction is smaller on C_χ than C_ϵ.

The overall trend in figure 13(*a*,*b*) does not, in spite of the scatter, rule out the possibility that the magnitude of $-n_u$ decreases towards 1 as the initial Reynolds number of the experiment increases. This Reynolds number is proportional to R_M for conventional passive grids, but is more correctly represented by the peak value of R_λ, $(R_{\lambda_u})_{max}$ immediately downstream of the grid, irrespectively of whether it is passive or active.

In particular, our analysis of the LD11 data for which the local value of R_{λ_u} reaches the largest value ($\simeq 1300$) obtained for grid turbulence suggests that $-n_u$ is close to 1 when R_{λ_u} approaches 1000. One should however keep in mind that, for the available passive and active grid data at large R_{λ_u}, the estimation of $-n_u$ is tainted

by various sources of uncertainty, arising mainly from the narrow range of x/M used and errors in the estimation of x_0 and $\langle\epsilon\rangle$. It would certainly be highly desirable to remedy this situation in future experiments. We should also note that the decrease of $-n_u$ with $(R_{\lambda_u})_{max}$ indicated in figure 13 confirms the observation of Burattini *et al.* (2006), based on a number of numerical simulations of decaying homogeneous isotropic turbulence, that $-n_u$ decreases towards one as $(R_{\lambda_u})_{max}$ increases.

For the present data, at small R_{λ_u}, the timescale ratio R is close to one. This value should also apply at larger R_{λ_u} provided the flow is heated in the same way. For passive grids with this type of heating, it would be reasonable to expect, for very large R_{λ_u}, complete self-preservation of the velocity and scalar fields (Speziale & Bernard 1992; Gonzalez & Fall 1998) with $n_u = -1$, $n_\theta = -R^{-1}$ or -1 (for $R = 1$). The corresponding invariants should then be

$$\langle\psi^2\rangle\lambda_\psi{}^2 = \text{constant}, \quad \langle\psi^2\rangle L_\psi{}^2 = \text{constant},$$

where $\psi \equiv u$ or θ.

Acknowledgement

The financial support by the Australian Research Council and 'Agence Nationale de la Recherche' is gratefully acknowledged.

REFERENCES

ANTONIA, R. A., BROWNE, L. W. B. & CHAMBERS, A. J. 1981 Determination of time constants of cold wires. *Rev. Sci. Instrum.* **52** (9), 1382–1385.

ANTONIA, R. A., LAVOIE, P., DJENIDI, L. & BENAISSA, A. 2010 Effect of a small axisymmetric contraction on grid turbulence. *Exp. Fluids* **49**, 3–10.

ANTONIA, R. A. & ORLANDI, P. 2004 Similarity of decaying isotropic turbulence with a passive scalar. *J. Fluid Mech.* **505**, 123–151.

ANTONIA, R. A., OULD-ROUIS, M., ANSELMET, F. & ZHU, Y. 1997 Analogy between predictions of Kolmogorov and Yaglom. *J. Fluid Mech.* **332**, 395–409.

ANTONIA, R. A., SMALLEY, R. J., ZHOU, T., ANSELMET, F. & DANAILA, L. 2003 Similarity of energy structure functions in decaying homogeneous isotropic turbulence. *J. Fluid Mech.* **487**, 245–269.

ANTONIA, R. A., SMALLEY, R. J., ZHOU, T., ANSELMET, F. & DANAILA, L. 2004 Similarity solution of temperature structure functions in decaying homogeneous isotropic turbulence. *Phys. Rev.* E **69**, 016305.

ANTONIA, R. A., ZHOU, T., DANAILA, L. & ANSELMET, F. 2000 Streamwise inhomogeneity of decaying grid turbulence. *Phys. Fluids* **12** (11), 3086–3089.

ANTONIA, R. A., ZHOU, T. & ZHU, Y. 1998 Three-component vorticity measurements in a turbulent grid flow. *J. Fluid Mech.* **374**, 29–57.

ANTONIA, R. A., ZHU, Y., ANSELMET, F. & OULD-ROUIS, M. 1996 Comparison between the sum of second-order velocity structure functions and the second-order temperature structure function. *Phys. Fluids* **8** (11), 3105–3111.

BATCHELOR, G. K. 1948 Energy decay and self-preserving correlation functions in isotropic turbulence. *Quart. Appl. Maths.* **6**, 97–116.

BATCHELOR, G. K. 1953 *The Theory of Homogeneous Turbulence*. Cambridge University Press.

BATCHELOR, G. K. & PROUDMAN, I. 1956 The large-scale structure of homogeneous turbulence. *Philos. Trans. R. Soc. Lond. Ser.* A **248** (949), 369–405.

BENNETT, J. C. & CORRSIN, S. 1978 Small Reynolds number nearly isotropic turbulence in a straight duct and a contraction. *Phys. Fluids* **21** (12), 2129–2140.

BIRKHOFF, G. 1954 Fourier Synthesis of Homogeneous Turbulence. *Commun. Pure Appl. Maths.* **7**, 19–44.

BROWNE, L. W. B. & ANTONIA, R. A. 1987 The effect of wire length on temperature statistics in a turbulent wake. *Exp. Fluids* **5**, 426–428.

BURATTINI, P., LAVOIE, P., AGRAWAL, A., DJENIDI, L. & ANTONIA, R. A. 2006 Power law of decaying homogeneous isotropic turbulence at low Reynolds number. *Phys. Rev.* E **73**, 066304.

BURATTINI, P., LAVOIE, P. & ANTONIA, R. A. 2005 On the normalized turbulent energy dissipation rate. *Phys. Fluids* **17**, 098103.

COMTE-BELLOT, G. & CORRSIN, S. 1966 The use of a contraction to improve the isotropy of grid-generated turbulence. *J. Fluid Mech.* **25** (4), 657–682.

CORRSIN, S. 1951 The decay of isotropic temperature fluctuations in an isotropic turbulence. *J. Aeronaut. Sci.* **18** (6), 417–423.

DANAILA, L., ANSELMET, F., ZHOU, T. & ANTONIA, R. A. 1999 A generalization of Yaglom's equation which accounts for the large-scale forcing in heated decaying turbulence. *J. Fluid Mech.* **391**, 359–372.

DANAILA, L., ANTONIA, R. A. & BURATTINI, P. 2004 Progress in studying small-scale turbulence using 'exact' two-point equations. *New J. Phys.* **6** (128).

DANAILA, L., ZHOU, T., ANSELMET, F. & ANTONIA, R. A. 2000 Calibration of a temperature dissipation probe in decaying grid turbulence. *Exp. Fluids* **28**, 45–50.

DAVIDSON, P. A. 2000 Was Loitsyansky correct? A review of the arguments. *J. Turbul.* **1** (6), 1–14.

DAVIDSON, P. A. 2009 The role of angular momentum conservation in homogeneous turbulence. *J. Fluid Mech.* **632**, 329–358.

FRISCH, U. 1995 *Turbulence: The Legacy of A. N. Kolmogorov*. Cambridge University Press.

FULACHIER, L. & ANTONIA, R. A. 1984 Spectral analogy between temperature and velocity fluctuations in several turbulent flows. *Intl J. Heat Mass Transfer* **27** (7), 987–997.

GEORGE, W. K. 1992*a* Self-preservation of temperature fluctuations in isotropic turbulence. In *Studies in Turbulence*, pp. 514–528. Springer.

GEORGE, W. K. 1992*b* The decay of homogeneous isotropic turbulence. *Phys. Fluids* **4** (7), 1492–1509.

GEORGE, W. K. & DAVIDSON, L. 2004 Role of initial conditions in establishing asymptotic flow behaviour. *AIAA J.* **42** (3), 438–446.

GONZALEZ, G. & FALL, A. 1998 The approach to self-preservation of scalar fluctuations decay in isotropic turbulence. *Phys. Fluids* **10**, 654–661.

HINZE, J. O. 1975 *Turbulence*. McGraw-Hill.

HUANG, M.-J. & LEONARD, A. 1994 Power-law decay of homogeneous turbulence at low Reynolds number. *Phys. Fluids* **6** (11), 3765–3775.

ISHIDA, T., DAVIDSON, P. A. & KANEDA, Y. 2006 On the decay of isotropic turbulence. *J. Fluid Mech.* **564**, 455–475.

KANG, H. S., CHESTER, S. & MENEVEAU, C. 2003 Decaying turbulence in an active-grid-generated flow and comparisons with large-eddy simulation. *J. Fluid Mech.* **480**, 129–160.

KÁRMÁN, T. & HOWARTH, L. 1938 On the statistical theory of isotropic turbulence. *Proc. R. Soc. Lond. Ser. A: Math. Phys. Sci.* **164** (917), 192–215.

KISTLER, A. L. & VREBALOVICH, T. 1966 Grid turbulence at large Reynolds numbers. *J. Fluid Mech.* **26** (1), 37–47.

KOLMOGOROV, A. N. 1941 On the degeneration of isotropic turbulence in an incompressible viscous fluid [also in 'Turbulence: Classical papers on statistical theory', 1961, Friedlander S. K. and Topper L. (Eds.), Interscience]. *Dokl. Akad. Nauk SSSR* **31**, 538–541.

KROGSTAD, P. Å & DAVIDSON, P. A. 2010 Is grid turbulence Saffman turbulence?. *J. Fluid Mech.* **642**, 373–394.

KROGSTAD, P. Å & DAVIDSON, P. A. 2011 Freely decaying, homogeneous turbulence generated by multi-scale grids. *J. Fluid Mech.* **680**, 417–434.

LARSSEN, J. V. & DEVENPORT, W. J. 2002 The generation of high Reynolds number homogeneous turbulence. In *Proceedings 32nd AIAA Fluid Dynamics Conference, Exhibit 2861*. AIAA Inc.

LARSSEN, J. V. & DEVENPORT, W. J. 2011 On the generation of large-scale homogeneous turbulence. *Exp. Fluids* **50**, 1207–1223.

LAVOIE, P. 2006 Effects of initial conditions on decaying grid turbulence. Ph.D. Thesis, University of Newcastle, Newcastle, Australia.

LAVOIE, P., DJENIDI, L. & ANTONIA, R. A. 2007 Effects of initial conditions in decaying turbulence generated by passive grids. *J. Fluid Mech.* **585**, 395–420.

LEE, S. K., BENAISSA, A., DJENIDI, L., LAVOIE, P. & ANTONIA, R. A. 2012*a* Decay of passive-scalar fluctuations in slightly stretched grid turbulence. *Exp. Fluids* **53**, 909–923.

LEE, S. K., BENAISSA, A., DJENIDI, L., LAVOIE, P. & ANTONIA, R. A. 2012*b* Scaling range of velocity and passive scalar spectra in grid turbulence. *Phys. Fluids* **24**, 075101.

LESIEUR, M. & OSSIA, S. 2000 3D isotropic turbulence at very high Reynolds numbers: EDQNM study. *J. Turbul.* **1** (7), 1–25.

LESIEUR, M. & SCHERTZER, D. 1978 Amortissement auto-similaire d'une turbulence à grand nombre de Reynolds. *J. Méc.* **17**, 609–646.

LLOR, A. 2011 Langevin equation of big structure dynamics in turbulence: Landau's invariant in the decay of homogeneous isotropic turbulence. *Eur. J. Mech.* B **30**, 480–504.

LOITSYANSKY, L. G. 1939 Some basic laws for isotropic turbulent flow [1945 English translation in Natl. Advis. Comm. Aeronaut. Tech. Memo. 1079]. *Trudy Tsentr. Aero.-Giedrodin Inst.* **440**, 3–23.

MAKITA, H. 1991 Realization of a large-scale turbulence field in a small wind tunnel. *Fluid Dyn. Res.* **8**, 53–64.

MANSOUR, N. N. & WRAY, A. A. 1994 Decay of isotropic turbulence at low Reynolds number. *Phys. Fluids* **6** (2), 808–814.

MOFFAT, R. J. 1988 Describing the uncertainties in experimental results. *Exp. Therm. Fluid Sci.* **1**, 3–17.

MOHAMED, M. S. & LARUE, J. C. 1990 The decay power law in grid-generated turbulence. *J. Fluid Mech.* **219**, 195–214.

MONIN, A. S. & YAGLOM, A. M. 1975 *Statistical Fluid Mechanics: Mechanics of Turbulence (vol. 2)*. MIT Press.

MYDLARSKI, L. & WARHAFT, Z. 1996 On the onset of high-Reynolds-number grid-generated wind tunnel turbulence. *J. Fluid Mech.* **320**, 331–368.

MYDLARSKI, L. & WARHAFT, Z. 1998 Passive scalar statistics in high-Péclet-number grid turbulence. *J. Fluid Mech.* **358**, 135–175.

PROUDMAN, I. & REID, W. H. 1954 On the decay of a normally distributed and homogeneous turbulent velocity field. *Philos. Trans. R. Soc. Lond. Ser. A Math. Phys. Sci.* **247** (926), 163–189.

REY, C., GENCE, J.-N., SCHON, J.-P. & MATHIEU, J. 1976 Étude de l'analogie entre champs thermiques et dynamique en turbulence homogène et isotrope dont les nombres de Péclet et de Reynolds sont petits, dans l'espace physique. *C. R. Acad. Sci. (Paris) Ser.* B **282**, 79–82.

RISTORCELLI, J. R. 2003 The self-preserving decay of isotropic turbulence: analytic solutions for energy and dissipation. *Phys. Fluids* **15** (10), 3248–3250.

SAFFMAN, P. G. 1967*a* Note on decay of homogeneous turbulence. *Phys. Fluids* **10**, 1349.

SAFFMAN, P. G. 1967*b* The large-scale structure of homogeneous turbulence. *J. Fluid Mech.* **27** (3), 581–593.

SCHEDVIN, J., STEGEN, G. R. & GIBSON, C. H. 1974 Universal similarity at high grid Reynolds numbers. *J. Fluid Mech.* **66** (3), 561–579.

SIRIVAT, A. & WARHAFT, Z. 1983 The effect of a passive cross-stream temperature gradient on the evolution of temperature variance and heat flux in grid turbulence. *J. Fluid Mech.* **128**, 323–346.

SPEZIALE, C. G. & BERNARD, P. S. 1992 The energy decay in self-preserving isotropic turbulence revisited. *J. Fluid Mech.* **241**, 645–667.

SREENIVASAN, K. R. 1984 On the scaling of the turbulence energy dissipation rate. *Phys. Fluids* **27** (5), 1048–1051.

SREENIVASAN, K. R. 1998 An update on the energy dissipation rate in isotropic turbulence. *Phys. Fluids* **10** (2), 528–529.

SREENIVASAN, K. R., TAVOULARIS, S., HENRY, R. & CORRSIN, S. 1980 Temperature fluctuations and scales in grid-generated turbulence. *J. Fluid Mech.* **100** (3), 597–621.

UBEROI, M. S. 1956 Effect of wind-tunnel contraction on free stream turbulence. *J. Aeronaut. Sci.* **23** (8), 754–764.

VALENTE, P. C. & VASSILICOS, J. C. 2011 The decay of turbulence generated by a class of multiscale grids. *J. Fluid Mech.* **687**, 300–340.

VALENTE, P. C. & VASSILICOS, J. C. 2012 Dependence of decaying homogeneous isotropic turbulence on inflow conditions. *Phys. Lett.* A **376**, 510–514.

VASSILICOS, J. C. 2011 An infinity of possible invariants for decaying homogeneous turbulence. *Phys. Lett. A* **375**, 1010–1013.

WANG, H. & GEORGE, W. K. 2002 The integral scale in homogeneous isotropic turbulence. *J. Fluid Mech.* **459**, 429–443.

WARHAFT, Z. & LUMLEY, J. L. 1978 An experimental study of the decay of temperature fluctuations in grid-generated turbulence. *J. Fluid Mech.* **88** (4), 659–684.

WYNGAARD, J. C. 1968 Measurement of small-scale turbulence structure with hot wires. *J. Sci. Instrum. (J. Phys.* E) **1**, 1105–1108.

WYNGAARD, J. C. 1969 Spatial resolution of the vorticity meter and other hot-wire arrays. *J. Sci. Instrum. (J. Phys. E)* **2**, 983–987.

ZHOU, T., ANTONIA, R. A., DANAILA, L. & ANSELMET, F. 2000 Transport equations for the mean energy and temperature dissipation rates in grid turbulence. *Exp. Fluids* **28**, 143–151.

ZHOU, T., ANTONIA, R. A., LASSERRE, J-J., COANTIC, M. & ANSELMET, F. 2003 Transverse velocity and temperature derivative measurements in grid turbulence. *Exp. Fluids* **34**, 449–459.